nature genetics

Mutations in the β-tubulin gene *TUBB2B* result in asymmetrical polymicrogyria

Xavier Hubert Jaglin[1,2,17], Karine Poirier[1,2,17], Yoann Saillour[1,2], Emmanuelle Buhler[3], Guoling Tian[4], Nadia Bahi-Buisson[1,2,5], Catherine Fallet-Bianco[6], Françoise Phan-Dinh-Tuy[1,2,16], Xiang Peng Kong[4], Pascale Bomont[7], Laëtitia Castelnau-Ptakhine[1,2], Sylvie Odent[8], Philippe Loget[9], Manoelle Kossorotoff[5], Irina Snoeck[10], Ghislaine Plessis[11], Philippe Parent[12], Cherif Beldjord[13], Carlos Cardoso[7], Alfonso Represa[7], Jonathan Flint[14], David Anthony Keays[15], Nicholas Justin Cowan[4] & Jamel Chelly[1,2]

Polymicrogyria is a relatively common but poorly understood defect of cortical development characterized by numerous small gyri and a thick disorganized cortical plate lacking normal lamination. Here we report *de novo* mutations in a β-tubulin gene, *TUBB2B,* in four individuals and a 27-gestational-week fetus with bilateral asymmetrical polymicrogyria. Neuropathological examination of the fetus revealed an absence of cortical lamination associated with the presence of ectopic neuronal cells in the white matter and in the leptomeningeal spaces due to breaches in the pial basement membrane. *In utero* RNAi-based inactivation demonstrates that *TUBB2B* is required for neuronal migration. We also show that two disease-associated mutations lead to impaired formation of tubulin heterodimers. These observations, together with previous data, show that disruption of microtubule-based processes underlies a large spectrum of neuronal migration disorders that includes not only lissencephaly and pachygyria, but also polymicrogyria malformations.

The crucial role of the tubulin superfamily in diverse cellular processes[1] and the association of *TUBA1A* mutations with a broad lissencephaly spectrum[2–4] led us to hypothesize that mutations in other tubulin genes that are highly expressed during central nervous system development might also result in malformations of cortical development. In a previous screen of individuals with agyria and pachygyria, we excluded *TUBA1B*, *TUBA1C* and *TUBB3* as candidate disease genes[3]. In this study, we report the screening of three additional candidate tubulin genes (*TUBB2A*, *TUBB2B* and *TUBB2C*) in individuals with a wide range of cortical dysgeneses, including polymicrogyria (PMG) syndromes associated with epilepsy and/or neurodevelopmental delay (see Methods). Although we did not find any nonsynonymous variations in either *TUBB2A* or *TUBB2C* (see alignment in **Supplementary Fig. 1** online), we found heterozygous missense mutations in *TUBB2B* (**Fig. 1a**) in four unrelated individuals and one fetus. All mutations (514T>C (S172P), 629T>C (I210T), 683T>C (L228P), 793T>C (F265L) and 935C>T (T312M)) affect residues that are rigidly conserved from yeast to human (**Supplementary Fig. 2** online) and reside in exon 4 (**Fig. 1a** and **Table 1**). Consistent with a *de novo* origin of the *TUBB2B* mutations, none were found in the parents of affected individuals or in 360 normal controls (see referenced polymorphisms in **Supplementary Fig. 1**).

Brain magnetic resonance imaging sequences showed that all individuals with *TUBB2B* mutations share the presence of a complex brain dysgenesis with bilateral, asymmetrical and anteriorly predominant PMG, fusion of the caudate and putamen with internal capsule hypoplasia, corpus callosum agenesis or dysgenesis and, in most cases, cerebellar and pons atrophy (**Fig. 1b–j**, **Table 1** and **Supplementary Fig. 3** online). In addition, neurohistopathological analysis of the fetal brain showed asymmetrical bilateral PMG with the absence of a corpus callosum, several nodular clusters of ectopic neurons in both hemispheres and a disorganization of cortical layering (**Fig. 1k–r**), including the presence of radial columnar heterotopic neurons in the white matter in the two hemispheres (**Fig. 1m**). These abnormalities strongly suggest migration defects and perturbations of axon tract formation associated with mutations in *TUBB2B*. In addition to

[1]Institut Cochin, Université Paris Descartes CNRS (UMR 8104), Paris, France. [2]Inserm, U567, Paris, France. [3]Plate-forme Post Génomique de l'INMED, INSERM U901, Parc scientifique de Luminy, Marseille, France. [4]Department of Biochemistry, New York University Medical Center, New York, New York, USA. [5]Service de Neurologie Pédiatrique, Département de Pédiatrie, Hôpital Necker Enfants Malades, AP-HP, Paris, France. [6]Service d'Anatomie Pathologique, Hôpital Sainte Anne, Paris, France. [7]Institut de Neurobiologie de la Méditerranée, INSERM U901, Parc scientifique de Luminy, Marseille, France. [8]Service de génétique médicale, CHU de Rennes-Hôpital Sud, Rennes, France. [9]Département d'anatomie et cytopathologie, CHU Pontchaillou, Rennes, France. [10]Locatie Juliana Kinderziekenhuis Polikliniek, Den Haag, The Netherlands. [11]Service de génétique, CHU Hôpital Clémenceau, Avenue Georges Clémenceau, Caen, France. [12]Département de pédiatrie et génétique médicale, CHU Hôpital Morvan, Brest, France. [13]Laboratoire de biochimie et génétique moléculaire, CHU Hôpital Cochin, Paris, France. [14]Wellcome Trust Centre for Human Genetics, University of Oxford, Oxford, UK. [15]Institute of Molecular Pathology, Vienna, Austria. [16]Present address: UMR-S 839, INSERM, Université Pierre et Marie Curie-Paris 6, Institut du Fer à Moulin, Paris, France. [17]These authors contributed equally to this work. Correspondence should be addressed to J.C. (jamel.chelly@inserm.fr) or N.J.C. (nicholas.cowan@med.nyu.edu).

Received 3 December 2008; accepted 9 March 2009; published online 24 May 2009; doi:10.1038/ng.380

the typical unlayered polymicrogyric cortex, analysis of the left hemisphere showed overmigration of MAP2-positive neurons through breaches in the pial basement membrane (**Fig. 1l**,**n**,**r** and **Supplementary Fig. 4** online). Analysis of radial glial fibers showed a marked disorganization beyond the pial basement membrane (**Fig. 1p**). These observations are reminiscent of the phenotype of mice inactivated for *Gpr56* (ref. 5), a gene associated with bilateral frontoparietal PMG in humans[6]. The macroscopic aspect and folding of the cerebellum appeared similar to the cerebellum of a control fetus of 27 gestational weeks. At the microscopic level, we observed many nodular heterotopia in both cerebellar hemispheres (data not shown).

To investigate the association between *TUBB2B* mutations and neuronal migration disorders, we studied the expression of *Tubb2b* during mouse brain development by *in situ* hybridization and qRT-PCR, and analyzed the consequences on the cortical neuronal migration of *TUBB2B* loss of function induced by *in utero* RNA interference. Sections of embryos at embryonic day 14.5 (E14.5) and 16.5 (E16.5) showed strong labeling restricted to central and peripheral nervous systems (**Supplementary Fig. 5** online). Using sagittal sections of the brain at E16.5, we found that expression predominated in the cortical plate and also within a thin layer in the subplate, whereas no signal was observed in the marginal zone and fainter labeling was seen in the ventricular and intermediate zones (**Supplementary Fig. 5a–e**). The strong labeling in the developing cortex subsequently decreased after birth, although *Tubb2b* labeling remained intense in the adult cerebellum, hippocampus and olfactory bulb (**Supplementary Fig. 5g**,**h**). Taken together, these data suggest that *Tubb2b* is strongly expressed in postmitotic neurons, with dominant expression during neuronal migration and differentiation[7–9], and to a lesser extent in progenitor cells. RT-PCR analysis also showed that *Tubb2b* is expressed in astroglial cells and C6 glial cells (data not shown).

We used a rat *in utero* RNAi approach[10] to knock-down *Tubb2b* expression by about 50% at E15.5, a time coincident with the migration of neurons within the cortex, to mimic the consequence of heterozygous loss-of-function mutations. We tested different small hairpin RNAs (shRNA) and used two shRNAs targeting either the coding sequence (CDS-sh) or the 3′ untranslated region (3′UTR-sh) that repressed *Tubb2b* expression *in vitro* by approximately 60%, whereas scrambled controls did not destabilize the *Tubb2b* mRNA

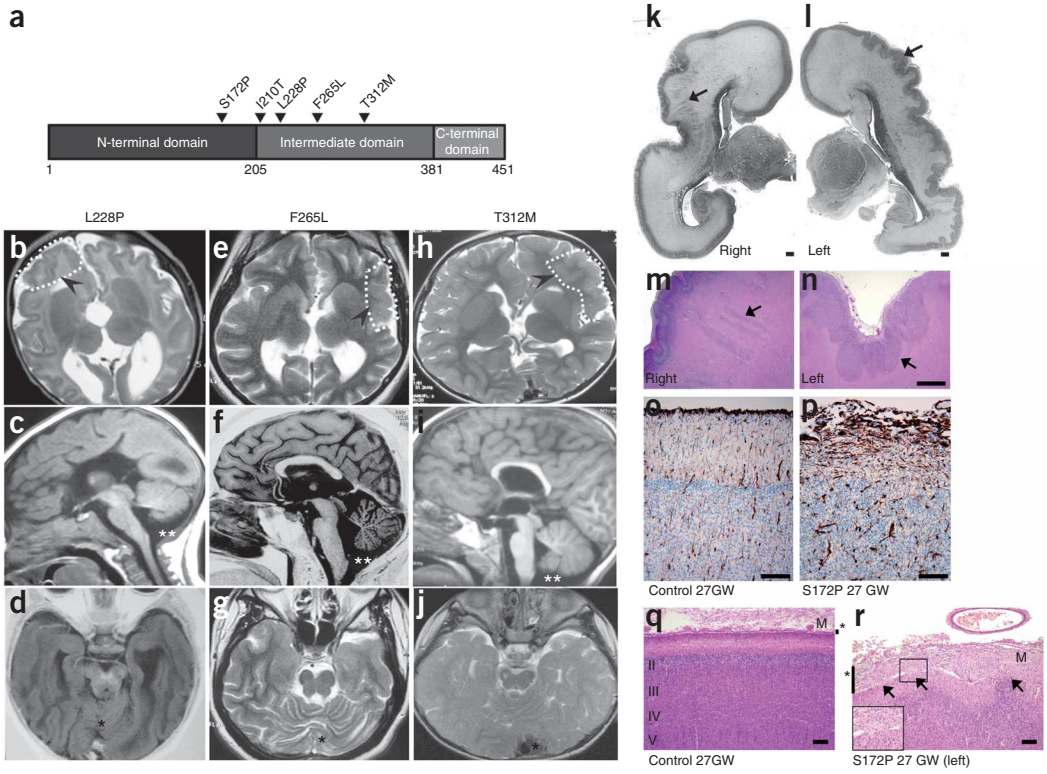

Figure 1 Magnetic resonance imaging and histopathology analyses of individuals with *TUBB2B* mutations. (**a**) Linear representation of the β-tubulin protein showing the position of heterozygous PMG-associated substitutions. (**b**–**j**) Representative brain imaging features of three individuals carrying *TUBB2B* substitutions: P2 (L228P) (**b**–**d**); P3 (F265L) (**e**–**g**); P1 (T312M) (**h**–**j**). Axial images show areas of PMG that appear more severe in frontal and parietal lobes (**b**,**e**) and involve the perisylvian region (**e**,**h**). The PMG appears either mildly (**b**,**h**) or severely asymmetric with left-sided predominance (**e**) (hatched lines highlighted by arrowheads show some of the PMG areas). Basal ganglia appear dysmorphic with a fusion of caudate and putamen and apparent absence of the anterior arm of the internal capsule (**b**,**e**,**h**). Midline sagittal section shows corpus callosum agenesis (**c**), hypogenesis and abnormal thickness (**f**) or dysmorphy with a flat shape (**i**) associated with mild to severe cerebellar vermis hypoplasia or atrophy (**c**,**f**,**i**) and with brainstem hypoplasia (double asterisks). Axial section at the level of the cerebellum and temporal lobes show severe vermian dysplasia (**d**,**j**) or atrophy (**g**) (black asterisks). (**k**–**r**) Nissl-stained sections of the 27GW fetus (S172P substitution) brain show asymmetrical bilateral polymicrogyria (black arrows in **k**,**l**) with callosal agenesis. Left and right hemispheres present respectively typical unlayered polymicrogyric cortex (**l**,**n**) and focal polymicrogyria with a completely disorganized cortex and radial neuronal heterotopias (black arrows in **k**,**m**). Several nodular heterotopic neuron clusters were also observed in both hemispheres. Sections of cortical regions of left hemisphere probed for vimentin (**o**,**p**) or stained by Nissl (**q**,**r**), respectively, show either abnormalities of radial glial fiber organization (**p**) or a disorganized cortex (**r**) with neuronal overmigration through the pial basement membrane (black arrows in **r**) into the leptomeningeal space (asterisks). Note differences of leptomeningeal space thickness. Sections (**o**,**q**) correspond to a 27-gestational-week control fetus. M, meninges. Scale bars: 500 μm (**k**–**n**), 100 μm (**o**–**r**).

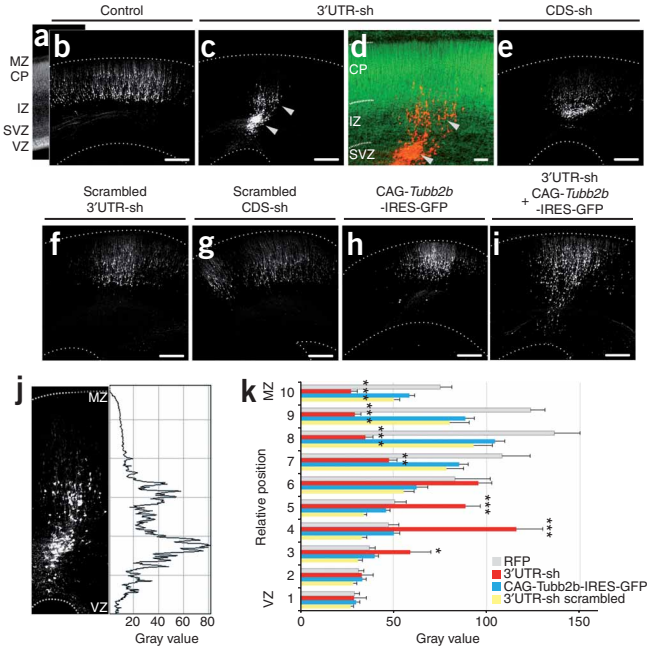

Figure 2 *In utero* knockdown of rat *Tubb2b* expression by RNAi alters neuronal migration in the isocortex. (**a**–**i**) Nissl staining on coronal sections of E20 brains reveals the overall organization of the cortex (**a**) 5 d after electroporation of a RFP-encoding reporter construct either alone (**b**) or in combination with 3′UTR-sh (**c**, overlay with Nissl in **d**), CDS-sh (**e**) or their corresponding scrambled controls (**f**,**g**). A rescue experiment was conducted using CAG-*Tubb2b*-IRES-GFP transfected either alone (**h**, GFP) or combined with 3′UTR-sh (**i**, GFP). (**j**,**k**) Fluorescence intensities reflecting cell positions were converted into gray values and measured across cortices from the VZ to the MZ (**j**, 3′UTR-sh). (**k**) Bars represent the mean ± s.e.m. of fluorescence intensities in ten strata dividing the thickness of cortices of independent brains (RFP $n = 5$, 3′UTR-sh $n = 6$, CDS-sh $n = 6$, scrambled 3′UTR-sh $n = 4$, scrambled CDS-sh $n = 5$, rescue $n = 6$). Knockdown of *Tubb2b* using both hairpins between E15 and E20 disrupts neuronal migration (**c**–**e**). RFP-positive cells are significantly stalled within the deep layers of the cortex (**c**,**k**, strata 4,5: $F(3,42) > 20.4$, $P < 0.0001$; $^{***}P < 0.001$ for 3′UTR-sh compared by Tukey-Kramer test to RFP, scrambled 3′UTR-sh and rescue, respectively) that correspond to the SV/IZ (**d**, higher magnification), whereas neurons have already reached the cortical plate in control conditions (**b**,**f**,**g**). *Tubb2b* overexpression preserves neuronal migration (**h**) showing that migration disruption is a specific consequence of *Tubb2b* RNAi as it rescued the defect (**i**,**k** strata 8–10: $F(3,42) > 23.7$, $P < 0.0001$, $^{***}P < 0.001$ for 3′UTR-sh compared by Tukey-Kramer test to RFP and rescue, respectively). $^{*}P < 0.1$ and $^{**}P < 0.01$, Tukey-Kramer test. Hatched lines in **b**,**c** and **e**–**i** correspond to the outer/ventricular limits of the cortex. Scale bars, 200 μm (**a**–**i**).

(**Supplementary Fig. 6a**,**b** online). These shRNAs combined with a red fluorescent protein (RFP)-encoding reporter construct were electroporated into progenitor cells located in the ventricular zone (VZ) of E15 rat neocortices. These cells give rise to further young neurons expressing the fluorescent protein as they migrate toward the cortical plate (**Fig. 2**). In E20 brain sections, we observed that neurons electroporated 5 days previously with RFP alone reached the cortical plate as expected (**Fig. 2a**,**b**). However, *in utero* expression of 3′UTR-sh induced a significant arrest of cells within the sub-ventricular zone (SVZ)/intermediate zone (IZ) (**Fig. 2c**,**d**,**j**,**k**; stratum 4: $F(3,42) = 21.716$, $P < 0.0001$; stratum 5: $F(3,42) = 20.394$, $P < 0.0001$). To further validate the specificity of our results, we carried out *in utero*

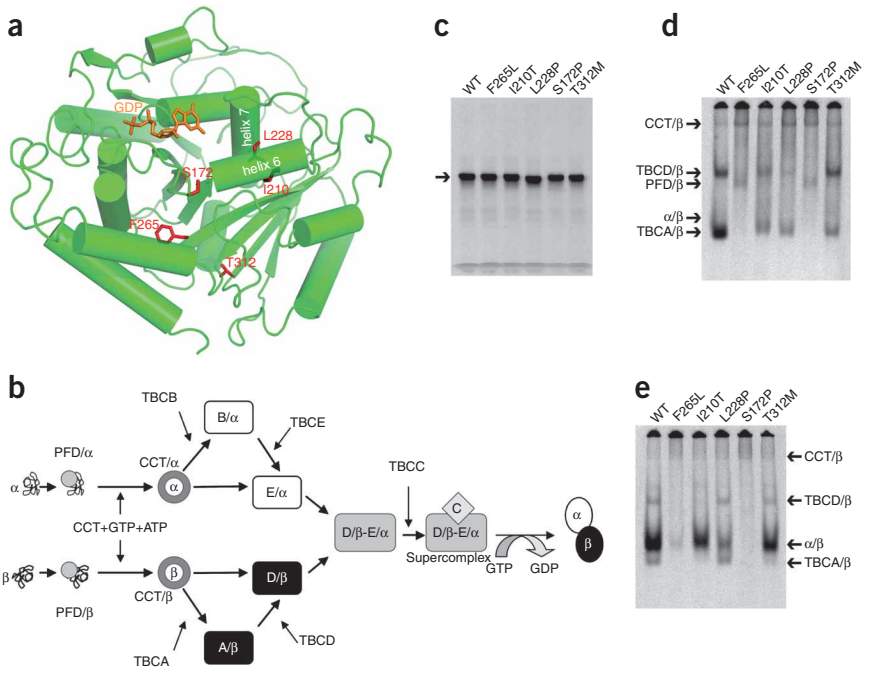

Figure 3 Various substitutions in TUBB2B result in inefficient α/β tubulin heterodimer formation *in vitro*. (**a**) Ribbon presentation illustrating placement of side chains of mutated residues (shown in red) and the E-site guanine nucleotide (shown in orange) within the structure of the β-tubulin polypeptide[11,12]. Ser172 resides between two proline residues in a loop. (**b**) The tubulin folding pathway involves a series of molecular chaperones whose function is to facilitate the assembly of the α/β tubulin heterodimer[25]. Newly translated α-tubulin (α) and β-tubulin (β) polypeptides are first captured and stabilized by prefoldin (PFD) that acts as a shuttling protein to deliver its bound target protein to the cytosolic chaperonin (CCT)[26]. CCT generates productive quasi-native folding intermediates which interact with a set of downstream tubulin-specific chaperones (TBCs)[27]. TBCB and TBCE capture CCT-generated α-tubulin intermediates in which the encapsulating GTP-binding pocket (the N-site) is already formed[28], producing TBCB/α-tubulin (B/α) and TBCE/α-tubulin (E/α) co-complexes. TBCA and TBCD capture and stabilize CCT-generated β-tubulin intermediates forming TBCA/β-tubulin (A/β) and TBCD/β-tubulin (D/β) co-complexes. TBCD/β-tubulin (D/β) and TBCE/α-tubulin (E/α) converge to form a supercomplex with TBCC (C-D/β–E/α). Interaction with TBCC (C) results in the triggering of GTP hydrolysis by β-tubulin[16]. This reaction acts as a switch to signal the release of newly formed GDP-bound α/β heterodimers, which are then competent for incorporation into microtubules. (**c**–**e**) Analysis by SDS-PAGE (**c**) or nondenaturing gels (**d**,**e**) of *in vitro* transcription-translation products conducted with wild-type (WT) and mutant TUBB2B and further chased with bovine brain tubulin to generate α/β tubulin heterodimers (**e**). The different migration pattern for L228P in **c** can be explained by the substitution of a proline in place of leucine, disrupting the helix, and presumably resulting in a change in the binding of SDS and hence a slight change in migration rate on the SDS gel. Note that F265L and S172P mutants yielded either only a trace or no discernable amount of α/β heterodimer. The remaining mutants all generated products present in the WT control, but in varying yield (**d**,**e**).

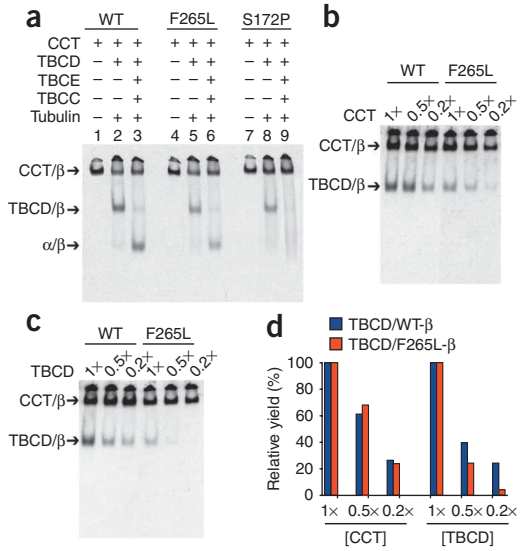

Figure 4 *In vitro* reactions reveal a lowered affinity of S172P TUBB2B for TBCD. (**a**) Analysis on nondenaturing gels of the products of reconstituted folding reactions containing ATP, GTP and various combinations of the purified components that are essential for the heterodimer assembly reaction. (**b**,**c**) Analysis on nondenaturing gels of the products of *in vitro* folding reactions performed with ^{35}S-methionine-labeled, unfolded wild-type (WT) or F265L mutant protein. Reactions contained a range of concentrations of purified cytosolic chaperonin (CCT) (1×, 0.5×, 0.2×) in the presence of constant (1× molar equivalent) TBCD (control reaction) (**b**) or a range of concentrations of purified TBCD (1×, 0.5×, 0.2×) in the presence of constant (1× molar equivalent) CCT (**c**). (**d**) Quantitation of the data shown in **b** and **c**. Note that when the abundance of TBCD was reduced by a factor of 5 in reconstituted reactions performed with a constant level of CCT, the yield of the TBCD–β-tubulin co-complex declined in the case of the wild-type protein to 25% of the original level, but declined to an undetectable level in the case of F265L. Similar data were obtained in the case of the S172P substitutions (**Supplementary Fig. 8**). The level of radioactivity present in complexes at the 1× concentration is taken as 100. Bars represent the average of two experiments. Arrows in **a–c** denote the migration positions of the CCT–β-tubulin binary complex, the TBCD–β-tubulin co-complex and the native tubulin heterodimer (α/β).

RNAi with the coding sequence CDS-sh and found that it led to the same migration arrest (**Fig. 2e** and **Supplementary Fig. 7** online). We also showed that the expression of both scrambled-sh controls did not disrupt migration (**Fig. 2f**,**g**). Finally, we conducted a rescue experiment in which we co-transfected a bicistronic construct driving the expression of Tubb2b and green fluorescent protein (GFP) as a reporter. Although the expression of this construct alone did not alter migration (**Fig. 2h**), it significantly suppressed the blocking effect of 3′UTR-sh on migration (**Fig. 2i**,**k**; strata 8–10: $F(3,42) > 23.4$, $P < 0.0001$). This RNAi-based approach reinforces the evidence that microtubules act as a critical node during corticogenesis and strongly implicates *Tubb2b/TUBB2B* in neuronal migration.

To define the functional consequences of the mutations in *TUBB2B*, we examined the potential effects of each of the mutated residues on the known structure of the β-tubulin polypeptide[11,12] (**Fig. 3a**). Ser172 resides in a loop that forms part of the guanosine nucleotide-binding site, which when mutated to a proline (S172P) is predicted to disrupt a hydrogen bond and to destabilize the GTP pocket. Leu228 and Phe265 are either in the vicinity of or part of the GTP/GDP binding site, with potential consequences for GTP binding. The remaining mutations seem to be less consequential in terms of GTP binding and overall protein stability. Because they are located on the surface, they may interfere with specific partner interactions.

We then investigated the ability of the β-tubulin mutants to produce functional α/β tubulin heterodimers through the complex chaperone-dependent folding pathway[13,14] (**Fig. 3b**) by transcription and translation in rabbit reticulocyte lysate[15]. All mutant proteins were translated as efficiently as a wild-type control (**Fig. 3c**). In contrast, analysis under native conditions showed a range of reaction products (**Fig. 3d**,**e**) that could be assigned on the basis of their electrophoretic mobilities[14,16]. In the case of TUBB2B mutant proteins, these products frequently differed both quantitatively and qualitatively from the wild-type control (**Supplementary Table 1** online). Most conspicuously, two mutant proteins (F265L and S172P) completely failed to yield the

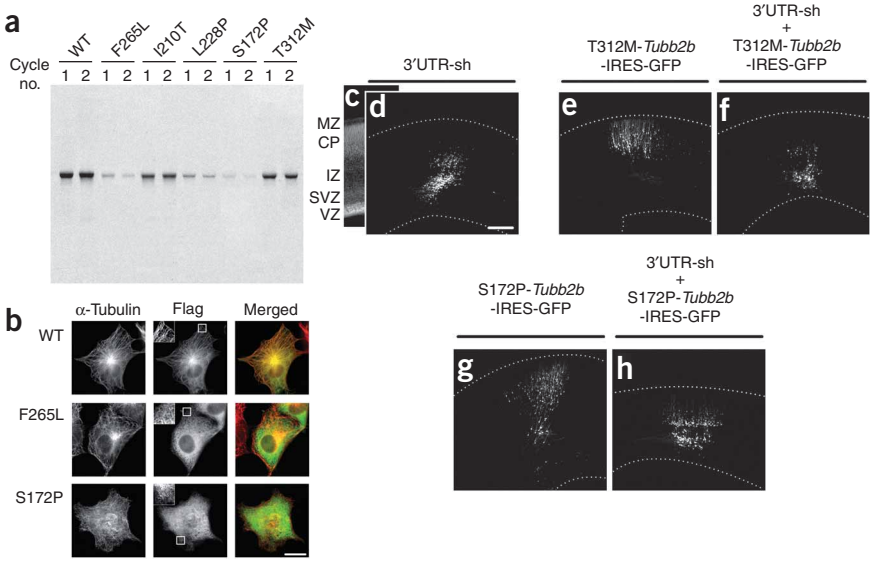

Figure 5 Loss of function of mutant TUBB2B *in vitro*, in cultured cells and *in vivo*. (**a**) Co-polymerization of labeled translation products with native bovine brain microtubules. Aliquots from two successive polymerization-depolymerization cycles (1 and 2) show inefficient incorporation for F265L, L228P and S172P mutants. (**b**) Expression of C-terminally Flag-tagged wild-type and mutant (S172P and F265L) TUBB2B *in vivo* after construct transfection into COS-7 cells. Note that F265L and S172P mutants do not incorporate into the microtubule network. (**c–h**) Nissl staining on coronal sections of E20 brains reveals the overall organization of the cortex (**c**) and repartition of GFP-positive cells within the E20 cortices thickness on coronal sections (**d–h**). Expression of T312M and S172P either alone (**e**,**g**) or in combination with 3′UTR-sh (**f**,**h**). Note that the overexpression of these mutants in combination with the hairpin does not rescue the neuronal migration defect caused by the RNAi (**d**,**f**,**h**), although the expression of each mutant alone does not lead to a major migration defect (**e**,**g**). However, we can see that upon expression of S172P a few cells seem to be blocked within the IZ, suggesting that S172P could have a dominant effect leading to slight migration impairments. Scale bars: 20 μm (**b**), 200 μm (**c–h**).

Table 1 Summary of clinical and imaging phenotypes associated with mutations in *TUBB2B*

Sex mutation	P1 Male 935C>T (T312M)	P2 Male 683T>C (L228P)	P3 Male 793T>C (F265L)	P4 Male 629T>C (I210T)	Male fetus 514T>C (S172P)
Age at last evaluation	2 years	2 years	37 years	13 years	27 weeks of gestation
OFC at birth (or brain weight at medical abortion)	33 cm	31 cm	31 cm	31 cm	Weight approximately 5th percentile
OFC at last examination (percentile)	45 cm (< −3 s.d.)	43.5 cm (< −3 s.d.)	51 cm (< −3 s.d.)	< −3 s.d.	NA
Motor/communication skills at last examination	Severe neuromotor impairment (tetraparesis); walks with aid, unskillful manipulation/limited language	Severe neuromotor impairment (tetraplegia); sits with aid, unskillful manipulation/no visual contact	No neuromotor impairment (no diplegia, no tetraplegia)/sentences, severe mental retardation	Severe neuromotor impairment (tetraparesis); walks with aid, unskillful manipulation/limited language	NA
Epilepsy	No seizures	Infantile spasms (3 months)	Generalized occasional seizures	Generalized seizures	NA
Gyral pattern	Polymicrogyria	Polymicrogyria	Polymicrogyria	Polymicrogyria	Polymicrogyria
Major location	Predominant in left frontal and parietal lobes	Predominant in frontal and temporal lobes (including the hippocampus)	Asymmetrical, predominant in left frontal, parietal and temporal lobes (including the hippocampus)	Asymmetrical, predominant in left frontal, parietal and temporal lobes	Bilateral and asymmetrical, fronto-temporal
Basal ganglia	Dysmorphic caudate and striatum	Dysmorphic caudate and striatum	Dysmorphic caudate and striatum	Dysmorphic caudate and striatum	Normal
Cerebellum	Vermian dysplasia	Vermian dysplasia with hypoplasia	Severe global atrophy	Vermian dysplasia with hypoplasia	Heterotopic neuronal cells
Corpus callosum	Flat shape and hypogenetic	Complete agenesis	Partial posterior agenesis	Atrophy and posterior agenesis	Agenesis
Brainstem	Mild hypoplasia predominant in pons	Mild hypoplasia	Hypoplasia predominant in pons	Hypoplasia predominant in pons	Normal

NA, not applicable; s.d., standard deviation.

intermediate corresponding to the co-complex of tubulin-specific chaperone A (TBCA) and β-tubulin (**Fig. 3d**,**e**). In addition, the yield of native α/β heterodimers produced following a chase with added native tubulin was either slightly reduced (in the case of I210T and T312M), markedly reduced (in the case of L228P and F265L) or undetectable (in the case of S172P) (**Fig. 3e**). (For kinetic analyses, see **Supplementary Note** and **Supplementary Fig. 8** online.)

To examine the mechanism of defective heterodimer assembly of the F265L and S172P mutant polypeptides in detail, we carried out reconstituted folding reactions *in vitro* using purified components[14,16]. We observed the generation of TBCD–β-tubulin co-complexes in reactions conducted with F265L and S172P (**Fig. 4a**) that might be ascribable to the relatively high concentrations of CCT and TBCD in these reactions compared to the more physiological concentrations in reticulocyte lysate. Indeed, when the abundance of TBCD was reduced by a factor of 5 in reactions conducted with a constant level of CCT, the yield of the wild-type β-tubulin–TBCD co-complex diminished to 25% of the original level, and the F265L β-tubulin–TBCD co-complex was reduced to an undetectable level (**Fig. 4b–d**). Similar data were obtained for the S172P substitution (**Supplementary Fig. 9** online). We conclude that, in addition to causing a marked failure of F265L and S172P CCT-generated folding intermediates to stably interact with TBCA, these mutations also result in a reduced efficiency of intermediate interaction with TBCD (**Supplementary Note** and **Supplementary Figs. 10** and **11** online). To assess the competence of mutant heterodimers expressed by transcription and translation to incorporate into microtubules, we analyzed their ability to co-cycle with native brain microtubules *in vitro* and to coassemble with microtubules upon transfection into cultured cells. In the cases of F265L and S172P, we observed a very low yield of labeled heterodimers incorporated into microtubules and a further diminution between the first and second cycles of polymerization and depolymerization, suggesting significant instability (**Fig. 5a**). Upon heterologous overexpression by transfection in cultured cells, we found that three mutants (I210T, L228P, T312M) behaved indistinguishably from the wild-type protein in that they were efficiently incorporated into interphase microtubules (data not shown). In contrast, in the case of the S172P and F265L mutants, there was scant evidence of incorporation into well-defined microtubules (**Fig. 5b**, see also **Supplementary Note** and **Supplementary Fig. 12** online for assessment of microtubule dynamics). Taken together, these experiments show that S172P and F265L are significantly compromised in their ability to properly assemble into microtubules *in vivo*, and are consistent with our *in vitro* transcription-translation experiments in which neither of these mutant proteins yielded significant amounts of polymerization-competent heterodimers (**Fig. 3e** and **Fig. 5a**).

We further sought to test whether expression of the S172P and unrelated T312M mutants *in vivo* could complement the phenotype caused by knockdown of *Tubb2b*. We electroporated the pCAGIG-S172P (or T312M)-*Tubb2b*-IRES-GFP construct either alone or in

combination with the 3′UTR-sh and analyzed the position of electroporated cells within the cortex (**Fig. 5**). We found that, although expression of each mutant alone does not massively affect migration (**Fig. 5e**,**g**), expression of each mutant in the knockdown context maintains the cells stalled within the SVZ/IZ (**Fig. 5f**,**h**) and fails to complement the RNAi effect (**Fig. 5d**).

In this study, we implicate mutations in *TUBB2B* as causative of brain malformations encompassing asymmetrical PMG associated with an unlayered cortex, heterotopic neuronal cells in the white matter and neuronal overmigration through the pial basement membrane. It is worth mentioning that corpus callosum dysgenesis, dysmorphic basal ganglia, cerebellum dysplasia and brainstem hypoplasia are common features of *TUBA1A*-related agyria/pachygyria and *TUBB2B*-related PMG. Mutations in *GPR56* and *SRPX2* genes are also known to be associated with PMG. However, the diagnosis of *TUBB2B*-related PMG could be evoked through assessment of clinical and imaging criteria highlighted in **Supplementary Table 2** online.

Our *in vitro* data show that the five newly discovered disease-associated *TUBB2B* mutations involve a spectrum of tubulin heterodimer assembly defects (summarized in **Supplementary Table 1**), leading to loss of function in the cases of S172P and F265L. The two most severe defects observed *in vitro* (S172P and F265L) are associated with the most and the least severe clinical phenotypes, respectively, suggesting that there is no simple correlation between *in vitro* and clinical phenotype among the five cases reported here. We also establish that loss of function is associated *in vivo* with defective migration and mislocalization of developing neurons within the cortex, suggesting that *TUBB2B*-related forms of PMG are primarily due to haploinsufficiency, though a dominant-negative effect cannot be excluded for the S172P substitution. For those mutations that have less or no apparent impact on tubulin heterodimer assembly, the functional defect seems likely to involve a subtle effect on either microtubule dynamics or on the interaction with one or more microtubule interacting proteins (MAPs) that are critical for proper cortical neuronal migration, or both. The cellular consequences of *TUBB2B* mutations and the mechanisms by which this results in PMG, an unlayered cortex and heterotopic neuronal cells remain unknown. We propose that the neuropathophysiology of *TUBB2B*-related PMG might result from a combination of both neuronal migration impairment and radial glia dysfunction that lead, respectively, to ectopic neurons in the white matter and cerebellum, and to pial membrane breaches (**Supplementary Note**).

In higher eukaryotes, α- and β-tubulins are encoded by a family of genes that are evolutionary conserved[17] among different species and differentially expressed[18,19]. To explain the need for these highly conserved multiple genes, it has been hypothesized that the different isotypes may be required to form specific sets of microtubules that carry out unique functions[18]. Although this hypothesis is still a matter of debate, our data showing that mutations in *TUBA1A* and *TUBB2B* are associated with different gyral abnormalities argue in favor of specific roles of *TUBB2B* and *TUBA1A* during corticogenesis and neuronal migration (**Supplementary Table 2**). It is also possible that subtle differences of spatio-temporal profiles of *TUBA1A* and *TUBB2B* expression (that is, populations of interneurons, radial glial cells and astro-glial cells) may account for some of the cortical phenotypic differences.

METHODS

Subjects and analysis of *TUBB2B*. We obtained DNA or blood samples and informed consent (from all parents) according to the guidelines of local institutional review boards at Cochin Hospital and INSERM (French National Institute of Health and Medical Research). *TUBB2B* was screened in 168 individuals with sporadic disease selected with clinical and brain imaging features compatible with a diagnosis of either lissencephaly ($n = 120$) or PMG syndromes ($n = 48$). Subjects with lissencephaly included those with agyria/pachygyria ($n = 105$) or subcortical laminar heterotopia ($n = 15$) with ($n = 13$) or without ($n = 107$) cerebellar hypoplasia or dysplasia. In addition, we also screened *TUBB2B* in five fetuses (using DNA samples derived from skin tissue) that had been sent to our diagnostic center after medical abortions and neuropathological analyses (**Supplementary Methods** online).

Neuropathological procedures. We carried out neuropathological analyses on five fetuses (aged from 23 to 35 gestational weeks) in accordance with French law. Briefly, after removal from the skull, each brain was fixed in 10% (v/v) formaldehyde solution containing NaCl (9 g/l) and $ZnSO_4$ (3 g/l) for a variable time (depending on the volume of the brain) from 3 to 6 weeks. Brains were cut in a coronal plane and sections involving one or both hemispheres were embedded in paraffin. Paraffin blocks were sectioned into either 5 μm (brainstem and cerebellum) or 8–10 μm (hemispheres) thick sections and stained using standard methods for histological and immunohistological studies.

RNAi constructs. We conducted RNAi experiments using two different oligonucleotides targeting the coding sequence or the 3′ UTR of rat *Tubb2b*: CDS-sh (318-341) and 3′UTR-sh (1553-1576). A BLAST search against databases confirmed the specificity of each target. Annealed oligonucleotides were cloned into a mU6-pro vector[20]. For the rescue experiment, we subcloned the coding sequence of *Rattus norvegicus Tubb2b* cDNA (IMAGE 5599369) without the UTRs into the pCAGIG vector[21] (Addgene plasmid 11159), such that a CMV immediate early enhancer/chicken β-actin promoter (CAG) drives transcription of the bicistronic *Tubb2b*-IRES-*GFP* mRNA. The rescue experiment allows the expression of a 3′ UTR targeting shRNA in combination with the overexpression construct. It implies that the overexpressed *Tubb2b* RNA is resistant to the shRNA as the target (3′ UTR) is absent.

***In utero* electroporation.** Wistar rats (Janvier, Le Genest Saint Isle, France) were mated, maintained and used in our animal facilities in agreement with European Union and French legislation. Timed pregnant rats (E15–E16; E0 was defined as the day of confirmation of sperm-positive vaginal plug) were anesthetized with ketamine and xylazine (respectively 0.1 and 0.01 mg per g body weight). The uterine horns were exposed and a lateral ventricle of each embryo injected via pulled glass capillaries and a microinjector (Picospritzer II; General Valve Corp) with Fast Green (2 mg/ml; Sigma) combined with the following DNA constructs: 0.5 μg/μl pCAGGS-red fluorescent protein (mRFP) either alone or with 1.0 μg/μl of shRNA construct targeting the *Tubb2b* mRNA. Plasmids were further electroporated by discharging a 4000 μF capacitor charged to 50 V with a BTX ECM 830 electroporator (BTX Harvard Apparatus). The voltage was discharged in five electric pulses at 950 ms intervals via 5 mm electrodes placed on the head of the embryo across the uterine wall. We conducted *in utero* electroporation in embryonic rats at E15.5. This moment corresponds to an active period of both radial and tangential migration of newborn neurons in the cortex.

Protein modeling. A model of human β-tubulin was built by homology modeling using available structures (Research Collaboratory for Structural Bioinformatics PDB code 1TUB) from Nogales *et al.*[11,12]. The image in **Figure 3a** was rendered using PyMOL.

***In vitro* translation.** Transcription-translation reactions were done at 30 °C for 60 min in 25 μl of rabbit reticulocyte lysate (TnT T7 Quick Coupled Transcription/Translation System, Promega) containing ^{35}S-methionine (specific activity 1,000 Ci/μmol; 10 μCi/μl) using TUBB2B wild-type and mutant cloned into the pET-23b(+) vector (Novagen) as templates. For the generation of labeled heterodimers, transcription-translation reactions were chased for a further 2 h at 30 °C by the addition of native bovine brain tubulin at 0.2 mg/ml. Labeled reaction products were detected by autoradiography after resolution on either SDS-PAGE or on native polyacrylamide gels as described[14,16].

***In vitro* folding reactions.** We conducted *in vitro* folding assays either directly in the rabbit reticulocyte translation cocktail or in folding buffer containing CCT (cytosolic chaperonin), ATP, GTP and tubulin chaperones (TBCB, TBCC, TBCD, TBCE) as described previously[16]. Target proteins (wild-type or mutant forms of TUBB2B β-tubulin) were expressed as ^{35}S-labeled proteins in *E. coli* BL21 DE3 pLysS cells[22] (Invitrogen) and the inclusion bodies purified and unfolded in denaturant following previously described procedures[23]. Reaction products were further analyzed by electrophoresis on native polyacrylamide gels[14,16]. In some experiments, the yield of various reaction products was determined using a phosphorimager (Personal Molecular Imager, Bio-Rad Laboratories).

Microtubule co-polymerization experiments. Products of *in vitro* translation reactions were mixed with depolymerized bovine brain microtubules and taken through successive cycles of polymerization and depolymerization as described[24]. At the end of each cycle, aliquots containing equal amounts of depolymerized material were removed and analyzed by SDS-PAGE and autoradiography.

Cell culture, transfections and immunofluorescence. Constructs were transfected into COS-7 cells grown on glass coverslips in DMEM containing 10% (v/v) FCS using the FuGENE6 transfection reagent (Roche Applied Science). Cells were fixed 24 h post-transfection with –20 °C methanol. Immunostaining was done with a polyclonal antibody to Flag (to visualize protein expressed from the construct; Sigma-Aldrich) and a monoclonal antibody to α-tubulin (to visualize the overall microtubule network; DM1A, Sigma-Aldrich).

Note: Supplementary information is available on the Nature Genetics website.

ACKNOWLEDGMENTS

We thank F. Francis for her helpful comments and critical readings of the manuscript, the subjects and their parents who contributed in this study and all the colleagues who provided clinical and imaging information. We thank R. Guerrini for providing us helpful advice. We are grateful to E. Leguern for allowing K.P. to develop this project and all the members of Cochin Institute genomic platform, Cochin Hospital Cell Bank, and Isabelle Souville for their technical assistance. This work was supported by funding from AP-HP, INSERM, FRM (funding within the frame of the Programme EQUIPEs FRM 2007) and ANR (ANR Neuro 2005, project A05183KS and ANR-06-NEURO-008-01 contract number RPV06055ASA). X.H.J. is supported by a PhD fellowship of the Ministère de l'Enseignement Supérieur et de la Recherche, by a grant for mobility from Université Paris Descartes and an EMBO short-term fellowship (ASTF 66.00-2008) for his work in NYU the Medical Center. K.P. is a post-doctoral researcher supported by FRM (Fondation pour la Recherche Medicale).

AUTHOR CONTRIBUTIONS

J.C. coordinated and instigated the study with D.A.K. and J.F. X.H.J. performed biochemical, cellular and *in vivo* functional studies. N.B.-B., K.P. and C.F.-B. recruited cases and controls. N.B.-B., C.F.-B., S.O., P.L., M.K., I.S., G.P., P.P. and C.B. helped in collecting patients. K.P., D.A.K. and Y.S. screened the subject DNAs and performed the genetic analyses. L.C.-P. performed all DNA extractions from subject samples and coordinated interaction with clinicians. C.F.-B. performed the neuropathological analyses. G.T. and N.J.C. provided reagents and expertise for the biochemical study; X.P.K. helped compute and analyze the structures; C.C., E.B., P.B. and A.R. provided expertise and technical assistance for *in utero* RNAi analysis. F.P.-D.-T. and K.P. performed the RNA *in situ* hybridization analysis. X.H.J. and K.P. drafted the manuscript with the help of N.J.C. and J.C.

Published online at http://www.nature.com/naturegenetics/
Reprints and permissions information is available online at http://npg.nature.com/reprintsandpermissions/

1. Dutcher, S.K. The tubulin fraternity: alpha to eta. *Curr. Opin. Cell Biol.* **13**, 49–54 (2001).
2. Keays, D.A. *et al.* Mutations in α-tubulin cause abnormal neuronal migration in mice and lissencephaly in humans. *Cell* **128**, 45–57 (2007).
3. Poirier, K. *et al.* Large spectrum of lissencephaly and pachygyria phenotypes resulting from *de novo* missense mutations in tubulin α 1A (*TUBA1A*). *Hum. Mutat.* **28**, 1055–1064 (2007).
4. Bahi-Buisson, N. *et al.* Refinement of cortical dysgeneses spectrum associated with *TUBA1A* mutations. *J. Med. Genet.* **45**, 647–653 (2008).
5. Li, S. *et al.* GPR56 regulates pial basement membrane integrity and cortical lamination. *J. Neurosci.* **28**, 5817–5826 (2008).
6. Piao, X. *et al.* G protein-coupled receptor-dependent development of human frontal cortex. *Science* **303**, 2033–2036 (2004).
7. Kriegstein, A.R. & Noctor, S.C. Patterns of neuronal migration in the embryonic cortex. *Trends Neurosci.* **27**, 392–399 (2004).
8. Marin, O. & Rubenstein, J.L. A long, remarkable journey: tangential migration in the telencephalon. *Nat. Rev. Neurosci.* **2**, 780–790 (2001).
9. Metin, C., Baudoin, J.P., Rakic, S. & Parnavelas, J.G. Cell and molecular mechanisms involved in the migration of cortical interneurons. *Eur. J. Neurosci.* **23**, 894–900 (2006).
10. Bai, J. *et al.* RNAi reveals doublecortin is required for radial migration in rat neocortex. *Nat. Neurosci.* **6**, 1277–1283 (2003).
11. Nogales, E., Whittaker, M., Milligan, R.A. & Downing, K.H. High-resolution model of the microtubule. *Cell* **96**, 79–88 (1999).
12. Nogales, E., Wolf, S.G. & Downing, K.H. Structure of the αβ tubulin dimer by electron crystallography. *Nature* **391**, 199–203 (1998).
13. Lewis, S.A., Tian, G. & Cowan, N.J. The α- and β-tubulin folding pathways. *Trends Cell Biol.* **7**, 479–484 (1997).
14. Tian, G. *et al.* Pathway leading to correctly folded β-tubulin. *Cell* **86**, 287–296 (1996).
15. Cleveland, D.W., Kirschner, M.W. & Cowan, N.J. Isolation of separate mRNAs for α- and β-tubulin and characterization of the corresponding in vitro translation products. *Cell* **15**, 1021–1031 (1978).
16. Tian, G. *et al.* Tubulin subunits exist in an activated conformational state generated and maintained by protein cofactors. *J. Cell Biol.* **138**, 821–832 (1997).
17. Little, M. & Seehaus, T. Comparative analysis of tubulin sequences. *Comp. Biochem. Physiol. B* **90**, 655–670 (1988).
18. Luduena, R.F. Are tubulin isotypes functionally significant. *Mol. Biol. Cell* **4**, 445–457 (1993).
19. Sullivan, K.F. & Cleveland, D.W. Identification of conserved isotype-defining variable region sequences for four vertebrate β tubulin polypeptide classes. *Proc. Natl. Acad. Sci. USA* **83**, 4327–4331 (1986).
20. Yu, J.Y., DeRuiter, S.L. & Turner, D.L. RNA interference by expression of short-interfering RNAs and hairpin RNAs in mammalian cells. *Proc. Natl. Acad. Sci. USA* **99**, 6047–6052 (2002).
21. Matsuda, T. & Cepko, C.L. Electroporation and RNA interference in the rodent retina *in vivo* and *in vitro*. *Proc. Natl. Acad. Sci. USA* **101**, 16–22 (2004).
22. Studier, F.W., Rosenberg, A.H., Dunn, J.J. & Dubendorff, J.W. Use of T7 RNA polymerase to direct expression of cloned genes. *Methods Enzymol.* **185**, 60–89 (1990).
23. Gao, M. & Knipe, D.M. Distal protein sequences can affect the function of a nuclear localization signal. *Mol. Cell. Biol.* **12**, 1330–1339 (1992).
24. Tian, G. *et al.* A pachygyria-causing α-tubulin mutation results in inefficient cycling with CCT and a deficient interaction with TBCB. *Mol. Biol. Cell* **19**, 1152–1161 (2008).
25. Cowan, N.J. & Lewis, S.A. Type II chaperonins, prefoldin, and the tubulin-specific chaperones. *Adv. Protein Chem.* **59**, 73–104 (2001).
26. Vainberg, I.E. *et al.* Prefoldin, a chaperone that delivers unfolded proteins to cytosolic chaperonin. *Cell* **93**, 863–873 (1998).
27. Spiess, C., Meyer, A.S., Reissmann, S. & Frydman, J. Mechanism of the eukaryotic chaperonin: protein folding in the chamber of secrets. *Trends Cell Biol.* **14**, 598–604 (2004).
28. Tian, G., Vainberg, I.E., Tap, W.D., Lewis, S.A. & Cowan, N.J. Quasi-native chaperonin-bound intermediates in facilitated protein folding. *J. Biol. Chem.* **270**, 23910–23913 (1995).